RSC Pharmaceutics

ROYAL SOCIETY OF CHEMISTRY

PAPER

View Article Online
View Journal | View Issue

Cite this: *RSC Pharm.*, 2025, **2**, 630

Comparative hygroscopic aerosol particle sizing measurements of the hygroscopic growth of inhaled pharmaceutical ingredients†

Yiliang Lance Jiang, [a] Josef Kadziola,[a] Jose R. Ruiz,[b] Richard Friend[b] and Jonathan P. Reid *[a]

Received 29th October 2024,
Accepted 18th March 2025

DOI: 10.1039/d4pm00310a

rsc.li/RSCPharma

The size distribution of an inhaled pharmaceutical aerosol generated by a nebulizer is a critical parameter influencing the deposition and therapeutic effect of the medication. Relative humidity (RH) can alter size distribution by promoting particle growth through condensation, depending on the hygroscopicity of the formulation. In this study, we evaluate the effect of RH on mannitol, trehalose, salbutamol, and tobramycin aerosols using the Comparative Hygroscopic Aerosol Particle Sizing (CHAPS) technique under varying RH conditions, ranging from ambient to physiological levels. The results demonstrate that RH significantly influences the aerosol particle size, with particle growth becoming more pronounced as RH exceeds 95%. The findings confirm that understanding the relationship between geometric radial growth factors (rGFs) from single droplet size measurements and the aerodynamic rGF is essential for more accurate prediction of plume size distribution, especially at lower RH levels. We also demonstrate consistency between the size distributions measured by CHAPS and a Next Generation Impactor (NGI), with CHAPS providing higher resolution in size and time and data on actuation-by-actuation variability in size distribution and aerosol dose.

1. Introduction

Nebulizers are considered a valuable tool for delivering therapeutic agents to the respiratory system. One of the primary advantages of nebulizers is that they require minimal coordination as the patient can inhale the mist during tidal breathing.[1] This can be contrasted with pressurized meter-dose inhalers and dry powder inhalers that require appropriate inhalation techniques. This ease of use is beneficial for patients with severe respiratory symptoms as well as those with limited coordination, such as children and elders. Another advantage of nebulizers is the ability to deliver high doses of medication,[2] invaluable for delivering drugs with low bioavailability or potency. By generating a continuous fine aerosol mist, nebulizers can deliver a substantial amount of the medication over an extended period directly to the target site within the lungs. Furthermore, nebulizers can deliver a wide range of formulations and active ingredients, including aqueous solutions, suspensions, proteins, and peptides, which may be susceptible to degradation or denaturation during the manufacturing processes required for pMDIs and DPIs, thereby offering a versatile platform for delivering fragile or sensitive therapeutic agents.[3,4] There are 3 main types of nebulizers: jet nebulizers, ultrasonic nebulizers and vibrating mesh nebulizers. While jet and ultrasonic nebulizers have their advantages, high residual volume and heating effects limit the efficient delivery of a wide range of medications.[5] Vibrating mesh nebulizers can significantly shorten the time for dose delivery while effectively aerosolizing suspensions, proteins, and liposomes.[5,6] In this study, we use a vibrating mesh nebulizer to actuate formulations of different compositions.

The efficacy of inhaled medications actuated from nebulizers is highly dependent on the droplet size distribution of the generated aerosol and how this evolves in the bolus during inhalation.[7,8] Comprehending and optimizing the aerodynamic characteristics and droplet size distribution are pivotal for enhancing drug delivery to the intended site while mitigating off-target deposition and side effects. It has been long known that the size distribution of pharmaceutical aerosols is affected by relative humidity (RH)[9] with the magnitude of the effect depending on the hygroscopicity of the ingredients within the formulation. The typical indoor RH level in homes across the United Kingdom ranges from 40% to 60%. However, the RH in the human respiratory system can reach above

[a]*University of Bristol, School of Chemistry, Cantock's Cl, Bristol, BS8 1TS, UK. E-mail: j.p.reid@bristol.ac.uk*
[b]*Chiesi Ltd, 1 Bath Road Industrial Estate, Bath Rd, Chippenham, SN14 0AB, UK*
† Electronic supplementary information (ESI) available. See DOI: https://doi.org/10.1039/d4pm00310a

99%.[10] Therefore, the aqueous solution aerosol generated by the nebulizer will dry out as the bolus mixes with ambient RH before experiencing a significant increase in RH while traveling through the respiratory system. The time span of drying can also vary. The traditional nebulizer tends to be connected to the patient *via* a mask, which allows a brief mixing of the bolus with the ambient air in between the patient's tidal breathing. Moreover, with the development of auxiliary tools that aid the delivery of inhaled medication, various equipment such as the universal spacer system manufactured by Inspiring Holdings Pty Ltd[11] allows more time for the plume generated from the nebulizer to equilibrate with ambient conditions prior to inhalation. Therefore, understanding how the distribution of particle sizes in the aerosol plume changes under different environmental conditions can provide meaningful insights into the deposition profile of the inhaled medication.

Using single particle characterization methods, such as the comparative kinetics-electrodynamic balance (CK-EDB) approach, the hygroscopicity of aerosol particles formed from nebulizer formulations can be extracted in the form of a radial growth factor (rGF) curve showing the variation in relative particle size with RH.[12] The measured growth factors can then be compared with model estimates, such as from the Aerosol Inorganic–Organic Mixtures Functional groups Activity Coefficients (AIOMFAC) model, which are often based on group contribution approaches to predict the extent of aqueous solvation of organic components with varying solution phase water activity. The water activity can be assumed equivalent to the surrounding RH for the aerosolized particles at equilibrium and of nebuliser size, *i.e.* for an RH of 50%, and the corresponding water activity would be 0.5. While single particle approaches provide detailed information on the idealised equilibrium response of inhaled aerosol, they do not provide information on the transient effects that may arise and impact size distribution during device actuation, the cooperative/interaction effects that occur between particles in a cloud and the variability in the delivered dose between actuations.

We have developed the Comparative Hygroscopic Aerosol Particle Sizing (CHAPS) approach to measure the aerodynamic size distribution of aerosolized particles generated by a nebulizer, soft mist inhaler or pMDI simultaneously at two RHs. For investigating the aerosol plume, CHAPS has a number of benefits over conventional methods such as Andersen cascade impactors and Next Generation Impactors, and over the idealised single particle approach. CHAPS provides high time resolution (of the order of 1 second) size distribution data allowing detailed characterization of the whole aerosol plume and providing insight into how the size distribution generated may vary across a single actuation. The relationship between the particle size distributions at two RHs can be immediately compared, and the absolute particle mass (including water content) can be routinely estimated allowing an examination of the reproducibility of aerosol delivery and the delivered dose over sequential device actuations. In all cases, CHAPS reports aerodynamic particle sizes, the size characterization appropriate for understanding the inhalation dynamics of the aerosol bolus. Finally, the phase behaviour of the aerosol (*e.g.* whether the aerosol is solution or crystalline in phase) can be inferred.

In this study, we investigate the dynamics of aerosol plumes of aqueous mannitol, trehalose, salbutamol, and tobramycin generated using a vibrating mesh nebulizer under varying RH conditions spanning from ambient to physiological levels. All these components are used for inhalation testing or treatment in patients,[13–16] and therefore would benefit from an in-depth understanding of how their deposition profile may be altered in the respiratory system due to RH. Additionally, we explore the consistency of single particle and plume size characterization approaches, providing insight into the timescale of water equilibration between the condensed and vapour phases.

2. Experimental

2.1. Single particle characterization and hygroscopic growth prediction

2.1.1. The comparative kinetic electrodynamic balance. The CK-EDB approach is used to obtain single droplet hygroscopic properties *via* experimentation. This method has been extensively described by Rovelli *et al.*,[17] so only a brief summary will be provided here. A solution sample (equivalent to that used in nebulizer formulations) is loaded into the reservoir of a droplet-on-demand (DoD) generator (MicroFab, MJ-ABP-01 30 μm orifice, USA). When combined with an annular induction electrode positioned a few millimetres in front of the DoD tip and held at a DC potential of typically between −80 and 80 V,[18] the DoD generator ejects charged droplets into the centre of the CK-EDB trapping chamber, where the droplets are levitated at the null point of the electrodynamic field between two pairs of concentric electrodes. A 532 nm laser beam illuminates the levitated droplet in the trap, and a CCD camera, centred at around 45° to the forward propagating direction of the beam, collects the elastic scattering from the droplet over an angular range of ±15°. The pattern of interference fringes from the light scattered by the droplet is referred to as the phase function.[19] If the particle is a homogeneous droplet, the droplet size can be estimated from the phase function and, specifically, the angular spacing of the interference fringes.[19] As the dispenser diameter is 30 μm, the initial radius of the droplet is approximately 26 to 30 μm. It should be noted that the physical size generated by the DoD dispenser is not within the ideal size range for inhalable medications. However, data obtained from the CK-EDB can be appropriately scaled and provide valuable information for predicting both the equilibrium properties and the dynamics of size change of smaller, respirable droplets.[20,21]

A second DoD generator produces probe droplets with a composition that has well-characterised hygroscopic response (*e.g.*, water or sodium chloride). Injected into the CK-EDB in sequence with nebulizer formulation solution droplets, the probe droplets can be used to estimate the exact RH within the chamber based on their evaporation kinetics.[22] Furthermore,

the temperature and RH of a gas phase flow are controlled and the flow introduced through the cylindrical electrodes into the CK-EDB, directly establishing the environmental conditions the droplet is exposed to. The RH can be set by adjusting the mixing ratio of dry and humidified nitrogen gas flows using mass flow controllers (Bronkhorst, the Netherlands), with the resulting flow passing over the trapped particle. The temperature of the gas phase in the trapping region is controlled by circulating ethylene glycol coolant through the electrode assembly, adjusting the gas flow temperature before it reaches the droplet trapping region.

As the CK-EDB approach relies on Mie theory for determining the particle size, estimates of the compositional dependence of the solution density and refractive index (and, thus, of the evaporating droplets as they change in size) are required. A parameterization of the solution density with a change in composition is obtained using a Densito density meter (Mettler Toledo, UK) with an accuracy of ±0.001 g cm^{-3}; refractive indices are measured using a Palm Abbe digital refractometer (MISCO, USA) with a precision of ±0.1 Brix. With these parameterisations, we can retrieve the hygroscopic response of our nebulizer formulations by measuring the equilibrium particle size at a range of RHs using an approach we have previously described in detail.[19] As the RH increases towards saturation (100%), the increase in equilibrated particle size becomes increasingly steep as the particle absorbs increasing amounts of water. For highly hygroscopic particles, we expect a significant increase in the radial growth factor (rGF) above that for less hygroscopic particles, with the exponential rise in rGF becoming significant at a lower RH. The droplet size estimated from the CK-EDB measurements is reported as an optical diameter, which can be assumed to be equivalent to the geometric diameter for spherical particles.[23] The hygroscopic growth can be obtained based on the droplet size retrieved at all time points during the evaporation event under a range of RH conditions.[24]

2.1.2. The AIOMFAC model and the interconversion of aerodynamic and geometric diameters. The Aerosol Inorganic–Organic Mixtures Functional groups Activity Coefficients (AIOMFAC) model[12] is a tool used to predict the thermodynamic properties of mixed inorganic–organic solution aerosols. The model allows the user to "build" an organic molecule based on its constituent chemical functional groups. Due to its extensive validation against experimental data for a wide range of functional groups,[25] AIOMFAC can predict water uptake and phase separation in aerosol particles under varying environmental conditions, reflecting the hygroscopic properties of aerosols.[26]

The relationship between the density and mass fraction of the solute (MFS), measured using a Densito density meter, can be converted into a density *vs.* relative humidity (RH) relationship. This conversion is based on predictions from the AIOMFAC model, which provides the water activity (equivalent to RH) as a function of MFS. The density information is crucial for converting a geometric rGF to an aerodynamic rGF, the size reported by the aerodynamic particle sizers used in CHAPS. Eqn (1) specifies the conversion from the geometric diameter (D_p) to the aerodynamic diameter (D_{ae}).

$$D_{ae} = D_p \sqrt{\frac{1}{\chi}\frac{\rho_p}{\rho_0}\frac{C_c(D_p)}{C_c(D_{ae})}} \quad (1)$$

As we are working with particles above 1 μm in diameter, the Cunningham slip correction (C_c) can be assumed to be 1 for both D_p and D_{ae}. The particle shape can also be assumed to be spherical with a dynamic shape factor (χ) of 1, provided the measurements are made at an RH at which the aerosol remains as aqueous droplets, *i.e.* is at an RH above the efflorescence point. By the definition of the aerodynamic diameter, ρ_0 equals 1 g cm^{-3}, the density of water, which leaves the density of the particle (ρ_p) the only factor influencing the conversion.

2.2. Plume characterization using the tandem aerodynamic particle sizer instrument

We have recently presented the development of CHAPS as a method to measure two aerosol size distributions from the same plume concurrently at two RHs using two aerodynamic particle sizers (model 3221, TSI).[27] The RH of the airflow that the aerosol from the nebulizer is first introduced into is controlled by adjusting the ratio of humidified and dry nitrogen gas flows using two mass flow controllers. The aerosol is then divided at a splitter into two paths at two RHs. The low RH environment is established by passing the aerosol through a Nafion dryer: the aerosol flows into an environment with a dry purge nitrogen gas flow, reducing the water content of the aerosol flow and the amount of condensed phase water in the plume. The intensity of drying can be adjusted by controlling the flow rate through the Nafion tube, allowing regulation of the RH entering APS_{dry}. The high RH environment for APS_{wet} is set by the RH of the initial conditioning flow that the plume is introduced into. On both the low and high RH flow paths, the aerosol passes into a spacer (volume of 0.5 L) that provides a mixing volume prior to aerosol sampling by the APS (at 5 L min^{-1}, *i.e.* at most a 6 s residence time in the spacer). The RH and temperature are measured in the spacers before the samples enter the two APSs.

The entire setup is mounted vertically on a frame to minimize the tube length and reduce bending and wall loss. To provide a flexible system and reduce costs, the parts of the CHAPS are 3D printed using a Raise3D Pro2 printer with a polylactic acid (PLA) filament for its water resistance. The 5 L min^{-1} airflow entering the APS is composed of a sheath flow of 4 L min^{-1} and a sample flow of 1 L min^{-1}. Particle velocity varies according to their aerodynamic diameters. As particles pass through two closely spaced laser beams, the time interval between their passage through each beam is measured, providing the particle's time of flight. Each recorded time-of-flight event corresponds to a single particle, allowing the APS to classify it into a specific size bin, as reported using Aerosol Instrument Manager 10.3 software (AIM, TSI Instrument, UK). The AIM software also estimates the mass of each particle based on its aerodynamic size and density. Summing all

recorded events over a 1-second interval provides the cumulative particle count or mass per second. The particle size distribution data exhibit a bimodal pattern, which is fitted using a custom Python script. A size-dependent correction factor is applied to the APS_{dry} to avoid differences in counting efficiency reflected in the two sets of APS results, potentially compromising any comparison at the two RHs.[27]

A MicroAir U100 (Omron, UK) nebulizer is used for the generation of the aerosol plume, and the entire CHAPS flow system is equilibrated to the target RHs before aerosol generation, also allowing the characterization of the baseline aerosol count. It takes approximately 12 minutes to actuate 5 mL of solution using the Omron U100 nebulizer. Assuming that the formulation is delivered at a steady pace throughout the plume generation, ~7 mg of solution is actuated per second from the device. For the CHAPS experiments, the length of aerosol generation is kept at 3 ± 1 seconds as the nebulizer requires manual initiation and termination. A short actuation avoids large RH fluctuations from the set points of the two flows.[27]

3. Results and discussion

3.1. Data extraction and processing

From the CHAPS measurements, we can visualize the plume development following each actuation at two different RHs. Fig. 1A and B present the typical evolving size distributions with a 1-second time resolution at 52% and 95% RH, respectively. The colour scale in Fig. 1 represents the particle count ($dN/d\log(D_p)$ cm^{-3}). Time 0 represents the start of sample recording on the AIM software, and ~15 s of background sample recording is collected for every run to ensure baseline consistency. An interesting observation is that, despite starting at the same time, the plume takes longer to dissipate at 95% RH (approximately 30 seconds) compared to 52% RH (approximately 25 seconds). Given the dynamic nature of the plume, the effect of varying environmental conditions is quantified and compared in a reproducible manner by averaging the first three seconds that no drastic changes in the size distribution are observed, or the "first three stable seconds". This choice is made because these early size distributions collected by the APS contain more particles in the larger size mode, a mode that is entirely within the detection range of the APS. As the plume develops, there is a shift towards a dominant mode with a smaller size distribution, part of which may fall below the detection limit (0.5 μm), leading to larger uncertainties in the fitted size distributions. Fig. 1C shows the size distributions of an actuation of 3% w/w mannitol during the first 3 stable seconds at 52% RH, clearly showing particles of smaller size than observed at a higher RH of 95% (Fig. 1D).

Bimodal size distributions are fitted to CHAPS particle size outputs generated from the nebulizer. Fig. 2A and B report bimodal distributions fit to the averaged first 3 stable seconds of the particle number concentration at 52% RH (Fig. 2A) and 95% RH (Fig. 2B) collected from a single actuation using CHAPS. The mean particle diameter of each mode can be extracted from the bimodal distribution fittings to calculate the *ratio between the rGFs* (rGFr) using eqn (2).

$$\mathrm{rGFr} = \frac{\mathrm{rGF}(\mathrm{RH_{high}})}{\mathrm{rGF}(\mathrm{RH_{low}})} \quad (2)$$

The diameter of the smaller size mode (mode 1) at a lower RH (1.252 ± 0.02 μm) is smaller than that at a higher RH (1.826 ± 0.50 μm), yielding an rGFr of 1.458 ± 0.430; the diameters of the larger size mode (mode 2) give an rGFr value of 1.390 ± 0.050. However, part of mode 1 in the low RH falls below the lowest size detection limit and, thus, mode 1 has a larger fitting error range at the high RH. Hence, the rGFr calculated with mode 2 provides the most accurate characterisation of the hygroscopic shift in size.

3.2. Hygroscopic plume dynamics for aerosolized aqueous mannitol

Mannitol was chosen as an exemplar of a water-soluble organic constituent with a hygroscopic response that can be measured by CHAPS and the CK-EDB approach, and modelled using AIOMFAC. Mannitol ($C_6H_{14}O_6$) is a six-carbon sugar alcohol (Fig. S1†) with 6 hydroxyl (–OH) groups, which allows for strong intermolecular hydrogen bonding networks.[28] It can be delivered to the patient through the pulmonary route[29] and is mainly used for two purposes: as a bronchial provocation test for assessing airway hyperresponsiveness in asthma[13] and as a maintenance treatment for cystic fibrosis patients.[30] In the bronchial provocation test, the patient inhales increasing doses of dry powdered mannitol before each spirometry test to challenge airway sensitivity. The degree of decline in lung function is used to help diagnose whether the patient is asthmatic.[13] Cystic fibrosis can be caused by a variety of gene mutations and often leads to the thickening of mucus and insufficient clearance of the airways.[9,10] The buildup of mucus results in a high prevalence of chronic bacterial infection, which requires medical intervention.[31,32] Currently, there is no cure for cystic fibrosis, but the symptoms can be alleviated by a range of treatment options, including a mannitol dry powder marketed as Bronchitol.[33] This treatment promotes osmosis of water into the airways, making the secretions less viscous and easier to remove. The patient has to pass a tolerance test before using the mannitol inhaler for cystic fibrosis treatment.[34] Nebulized mannitol is also being explored for the treatment of cystic fibrosis for children.[35]

3.2.1. Single particle hygroscopic growth characterization and prediction. The rGF value at different RHs can be obtained experimentally using the CK-EDB or predicted using the AIOMFAC model, with both methods ultimately providing quantification of the change in geometric radius with RH. The AIOMFAC-derived geometric growth factor (rGF_{geo}) can be converted to aerodynamic rGF (rGF_{aero}) using eqn (1). A Densito density meter enables the determination of the experimental correlation between the density and the mass fraction of aqueous mannitol (Fig. S2†). Since AIOMFAC provides an esti-

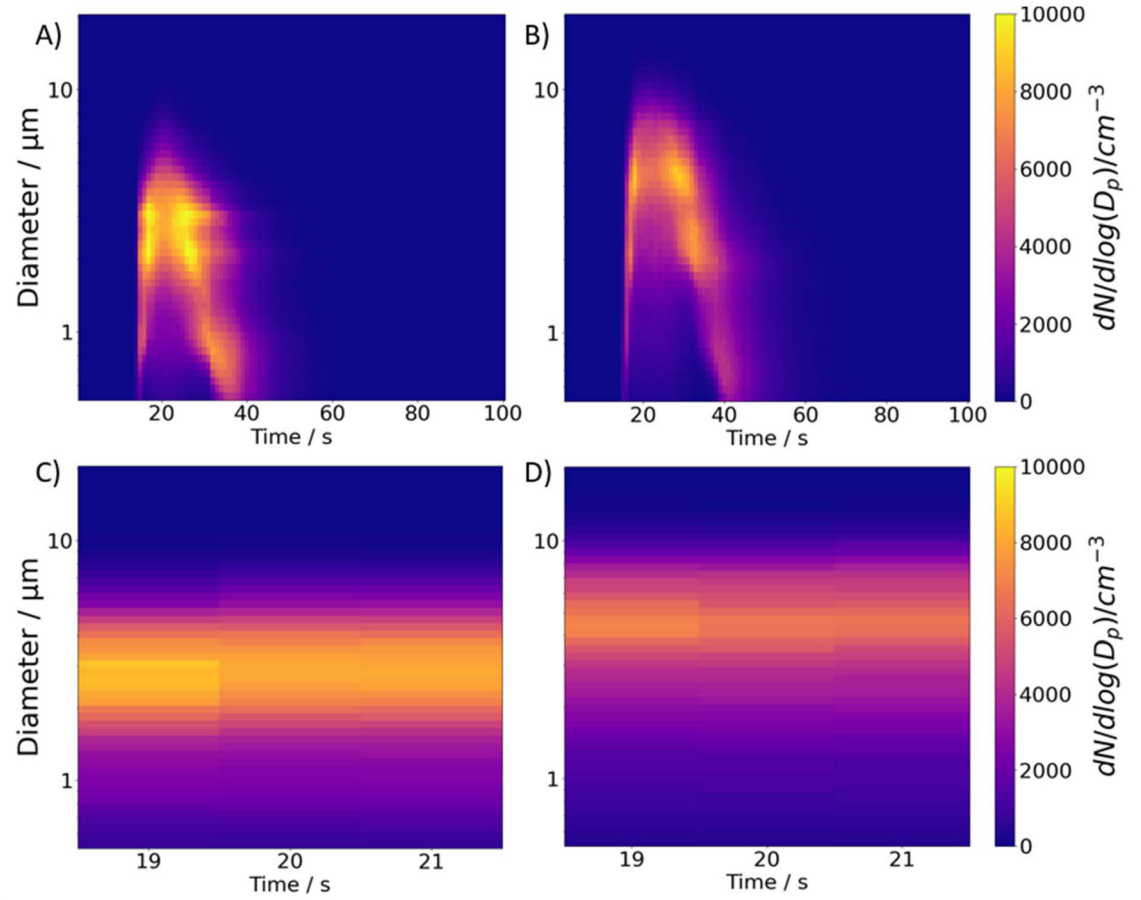

Fig. 1 Plume development in an initial formulation of 3%w/w mannitol actuated from a nebulizer over 3 seconds of actuation at (A) 52% RH in APS_{dry} and (B) 95% RH in APS_{wet}. (C) and (D) show the first 3 stable seconds for lower and higher RH, respectively.

mate of the relationship between the RH and solute mass fraction, the corresponding density can be applied to convert rGF_{geo} to rGF_{aero} at the measurement RH. The correction for density does not significantly impact the mannitol rGF curve above 95% RH (Fig. S3†), as the MFS is low and the particle is mainly water with a density close to 1 g cm^{-3}. However, an increasing deviation in the two rGF values occurs at lower RHs as the MFS increases.

The CK-EDB data are in good agreement with the AIOMFAC predictions in the dilute limit especially above 0.9 water activity, or 90% RH (Fig. S3†). Minor differences can be observed when the RH drops below 90% for CK-EDB and AIOMFAC curves. From the EDB phase function output in Fig. S4,† it is observed that the droplet becomes crystalline upon equilibration at 40–50% RH. At 70% RH, the droplet remains homogeneous after evaporation and equilibration. In between these limits at an RH of 60%, the aqueous mannitol droplet is first homogeneous upon equilibration, but resembles a core–shell structure or has inclusions after it has been levitated for over 12 seconds (Fig. S4†), suggesting that some phase separation or partial crystallisation occurs.[19] The equilibrated radius at 70% RH is just over 10 µm, which is slightly higher than the radius at 60% RH, which is just below 10 µm. The phase behaviour and non-ideal mixing become more pronounced at low water contents.

3.2.2. CHAPS plume characterization. Obtaining the relationship between water activity and the mass fraction of solute from the AIOMFAC model is crucial for the conversion to the aerodynamic rGF from the geometric rGF. However, AIOMFAC has limitations in terms of the functional groups (and, hence, molecules) that can be modelled. Hence, it is informative to compare rGFr values measured by CHAPS with calculated values based on both geometric and aerodynamic rGFs for systems that can be fully represented by AIOMFAC, in order to establish the extent of the difference. The extent to which AIOMFAC represents the CHAPS measurements should also be compared with expectations from the CK-EDB measurements. Thus, we can still assess if the plume data and single particle data are in agreement for substances where we cannot obtain the aerodynamic rGFr ($rGFr_{aero}$).

The CHAPS $rGFr_{aero}$ of a 3% w/w aqueous mannitol formulation in the nebulizer is compared to the $rGFr_{geo}$ derived from the CK-EDB output in Fig. 3A. The data points in Fig. 3A are expected to align with the line representing a gradient of 1 if

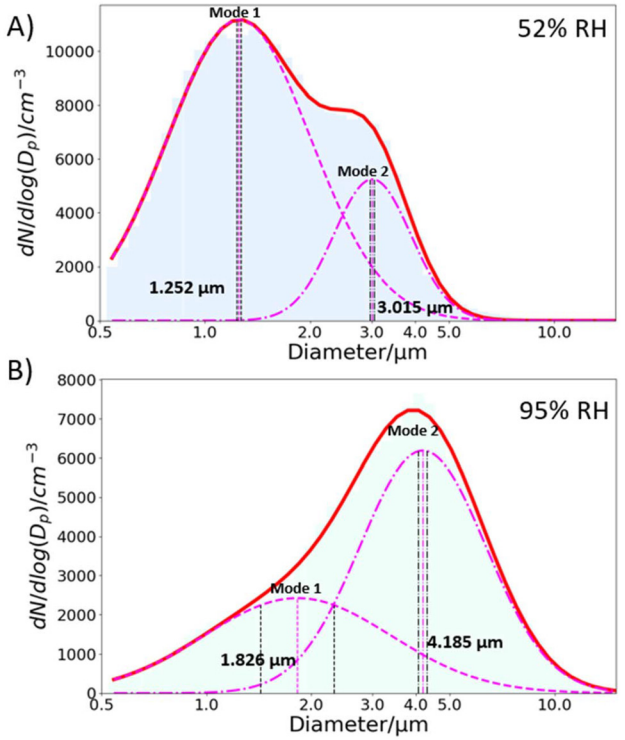

Fig. 2 3%w/w mannitol CHAPS results in the first 3 stable seconds for (A) 60 ± 1% RH in APS_{dry} with a mode 1 value of 1.252 ± 0.02 μm and a mode 2 value of 3.015 ± 0.040 μm and (B) 95 ± 1% RH in APS_{wet} with a mode 1 value of 1.826 ± 0.50 μm and a mode 2 value of 4.185 ± 0.105 μm. The light blue and light green in the background are the raw CHAPS results for APS_{dry} and APS_{wet}, respectively. The vertical black dashed lines alongside the mode (vertical pink dashed lines) represent the uncertainty of the bimodal fit.

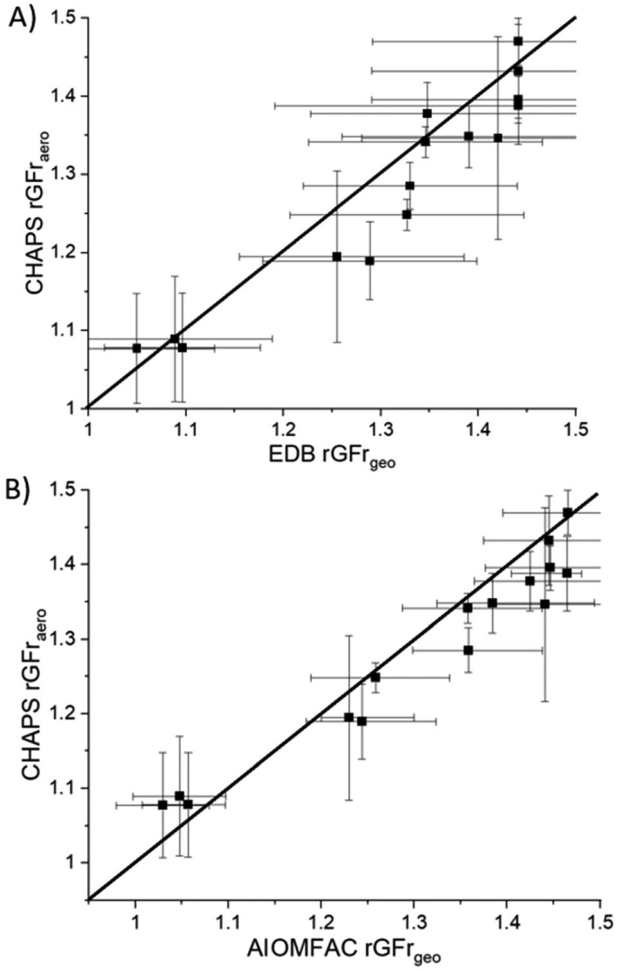

Fig. 3 Comparison between the CHAPS $rGFr_{aero}$ of aqueous mannitol and geometric rGFr obtained from EDB (A) and AIOMFAC (B). The black line has a gradient of 1. The error bar for the CHAPS $rGFr_{aero}$ is based on the error range of the bimodal fitting and the error bar for the $rGFr_{geo}$ is based on the uncertainty in the RH sensors.

the hygroscopic growth measurements made on the plume and single particles are consistent. Such agreement would also indicate that the particle sizes in the plume are fully equilibrated at the RH of the measurement. For RHs below 90%, the sensor uncertainty is ±1%, increasing to ±1.7% at RHs above 90%. However, due to consistent and reproducible size distribution data in the 95%+ RH range from APS_{wet},[27] an RH uncertainty of ±1% is included in our analysis for values above 90%. This uncertainty is used to calculate the error bar for EDB $rGFr_{geo}$. For instance, if 95% RH is maintained in APS_{wet} and 60% RH in APS_{dry}, the upper error limit for EDB $rGFr_{geo}$ is calculated by dividing the rGF_{geo} at 96% by that at 59% RH, while the lower error limit is determined by dividing the rGF_{geo} at 94% by that at 61% RH, as demonstrated in eqn (2). The error bar for EDB $rGFr_{geo}$ remains large because of the exponential increase in rGF at high RH (Fig. S3†). The uncertainty in CHAPS $rGFr_{aero}$ stems from the error associated with the bimodal fit, as demonstrated in Fig. 2.

To obtain a range of rGFrs as shown in Fig. 3A, the RH in APS_{wet} is set to 95% ± 1%, while the RH in APS_{dry} is increased from 50% to 90% in 10% increments by varying the flow rate of the drying nitrogen. When APS_{dry} reaches a high RH (90%), the mode mean size of the largest peak of APS_{wet} and APS_{dry} size distributions are in close agreement, resulting in an rGFr value that is close to 1. Fig. 3B shows a comparison of the $rGFr_{geo}$ calculated from the AIOMFAC-derived rGF_{geo} curve (Fig. S3†) with measurements using the CHAPS data, showing a similar level of agreement to the EDB $rGFr_{geo}$ results (Fig. 3A).

Since the correlation between the RH and mass fraction of mannitol can be modelled using AIOMFAC, the density parameterization can be applied to the corresponding mass fraction of mannitol to convert rGF_{geo} to rGF_{aero}. Fig. 4 shows a comparison of the density adjusted AIOMFAC $rGFr_{aero}$ with the CHAPS $rGFr_{aero}$. As seen in Fig. S3,† the density adjusted rGF_{aero} is higher than the rGF_{geo}, particularly at a lower RH level, which increases the rGFr when the RHs for APS_{wet} and APS_{dry} are most disparate. When the RH of the airflow feeding into APS_{dry} is low (*i.e.* 50%), the mass fraction of mannitol becomes higher due to the reduced water content, amplifying the impact of the density correction. Consequently, while both

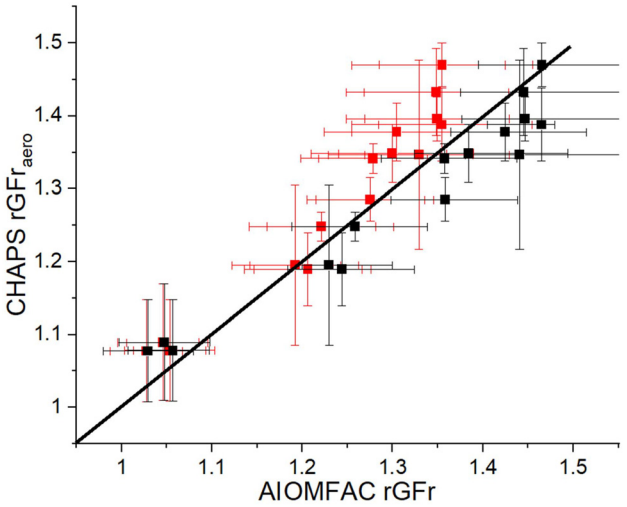

Fig. 4 Comparison between the CHAPS rGFr$_{aero}$ of aqueous mannitol and AIOMFAC rGFr$_{aero}$ (red) with AIOMFAC rGFr$_{geo}$ (black) as a reference. The black line has a gradient of 1.

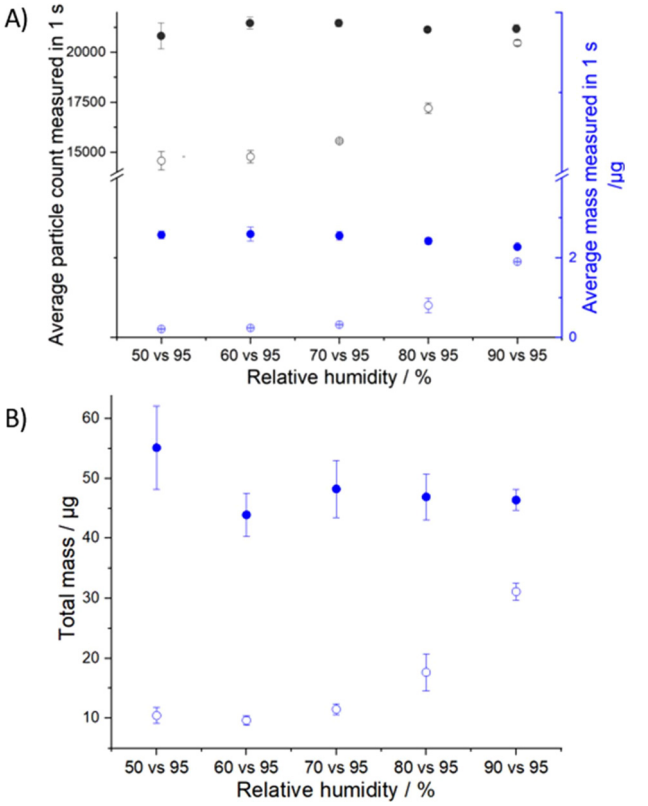

Fig. 5 (A) 3%w/w mannitol CHAPS results with 3 seconds of actuation for a range of RHs in the APS$_{dry}$ from 90% down to 50%, while maintaining around 95% ± 1% in the APS$_{wet}$ (n = 3 for each RH pair). The black symbols show the average particle count of the samples over 3 seconds. The blue symbols show the average mass over those 3 seconds. APS$_{dry}$ data are presented using open dots, while APS$_{wet}$ data are presented using filled dots. The error bars represent the standard error of the mean (SEM) from the 3 repeats. (B) Graph showing the cumulative mass of mannitol throughout the entire actuation APS$_{dry}$ shown in open dots and APS$_{wet}$ in filled dots. The error bars represent the SEM based on n = 3 for each data point.

AIOMFAC rGFr$_{geo}$ and rGFr$_{aero}$ show reasonable consistency with CHAPS measurements, the level of agreement between them decreases as the disparity in density increases (*i.e.* as the RH of APS$_{dry}$ decreases). This trend suggests that the density correction may not fully account for the change in aerodynamic size under low RH conditions. Future work will focus on investigating the impact of such RH and density disparities to improve the consistency between single particle rGFr$_{geo}$, rGFr$_{aero}$, and CHAPS rGFr$_{aero}$ under a wider range of conditions. As there are limitations in the molecular functional groups that can be represented in AIOMFAC, we will primarily focus on comparing CHAPS measurements with CK-EDB rGFr$_{geo}$ measurements in this paper. By concentrating on this comparison, we aim to assess the consistency between CHAPS and the well-established CK-EDB method for analyzing aerosol growth factors, while avoiding potential uncertainties associated with density parameterization and AIOMFAC's model limitations.

Fig. 5 reports the average cumulative particle count and mass per second over the 3 stable seconds. During the experiment, the RH in APS$_{wet}$ is maintained at 95%. Under the same RH conditions, the average particle count reproducibly measured is around 21 000 particles per second over the stable 3-second interval (Fig. 5A). The APS$_{dry}$ instrument records a lower average particle count and mass than the APS$_{wet}$ throughout the experiment, especially at lower RHs. The lower particle count is most likely due to undercounting of particles in the APS$_{dry}$ channel with a larger proportion of particle sizes below the detection limit (300 nm) at low RH. When the RH is between 50% and 70%, the APS$_{dry}$ records an average particle count of around 15 000 particles per second. Within this RH range, the expected aerodynamic rGF values are very close (consistent with Fig. S3†), reflecting that the particle radii do not undergo significant growth. The particle count in APS$_{dry}$ increases as the RH increases: at 90% RH, the average particle count is ~20 000 particles per second, close to that of the APS$_{wet}$ (Fig. 5A). The rise in the particle count in APS$_{dry}$ suggests that as the particles grow with RH, a larger fraction surpass the size detection limit.

The cumulative mass delivered in APS$_{wet}$ in 1 second remains just over 2 μg at 95% RH and shows good reproducibility (Fig. 5A). For APS$_{dry}$, the similarity in the rGF across the range of dry RHs means that the average mass measured per second within this RH range remains similar (Fig. 5A). As the RH in APS$_{dry}$ increases to 80% and 90%, the average mass also increases exponentially due to hygroscopic growth, approaching that in APS$_{wet}$.

The total mass of a single actuation entering the APS can be calculated by summing the cumulative mass per second over the entire sampling period. The total mass of aerosolized mannitol droplets measured with the APS$_{wet}$ instrument over the 3-second plume actuation period ranges between 45 μg and 55 μg (Fig. 5B). The variability associated with the mass

measurements may arise from the manual process of initiating and terminating plume generation, which can lead to small inconsistencies in the precise duration of each actuation. At RH levels between 50% and 70%, the total cumulative mass measured by the APS_{dry} instrument does not exhibit significant changes. However, a pronounced increase in mass can be found at higher RH conditions of 80% and 90%, again approaching that in APS_{wet}.

3.3. Hygroscopic plume dynamics for aerosolized aqueous trehalose

Trehalose is a non-reducing disaccharide composed of two glucose units linked by a glycosidic bond (Fig. S5†).[36] According to Richards *et al.*,[37] trehalose in its pure form has low hygroscopicity. However, by methods such as spray drying, trehalose can become amorphous and have altered properties, including enhanced hygroscopicity.[16] The 5% w/w trehalose solution prepared for this experiment uses the pure form.

3.3.1. Single particle characterization and prediction. The AIOMFAC rGF_{geo} curve and CK-EDB rGF_{geo} curve are depicted in Fig. S6.† The model predictions align closely with the experimentally obtained rGF values. At a lower water activity (0.6–0.85), trehalose exhibits a gradual increase in the rGF gradient, with a more pronounced increase observed at water activity levels above ~0.95. Green[38] demonstrated that trehalose droplets remain homogeneous at 60% RH, according to the CK-EDB phase function output.

3.3.2. CHAPS plume characterization. Following the procedure for mannitol, Fig. 6 shows a comparison of CHAPS $rGFr_{aero}$ with CK-EDB $rGFr_{geo}$. As expected, the error bar remains substantial since APS_{wet} is maintained at 98 ± 1% RH. The RH in APS_{dry} is increased from 60% to 80% in 10% increments. The data points in Fig. 6 are located close to the line gradient unity, which suggests that CK-EDB and CHAPS show good agreement.

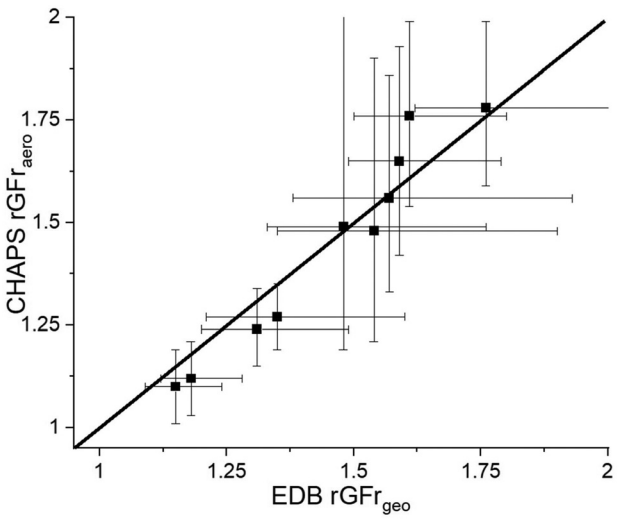

Fig. 6 Comparison between the CK-EDB $rGFr_{geo}$ of aqueous trehalose and the CHAPS $rGFr_{aero}$.

Fig. 7A presents the cumulative particle count and mass of trehalose during the first 3 stable seconds of CHAPS output. The APS_{wet} humidity conditions are maintained at 98 ± 1%, with a consistent average particle count of approximately 23 000 particles per second observed over the stable 3-second interval (Fig. 7A). As the RH in APS_{dry} increases from 60 ± 1% to 80 ± 1% RH, the particle count also rises from ~10 000 particles to ~23 000 particles with the number tending towards that measured by APS_{wet}. This trend is attributed to hygroscopic growth, leading to a greater number of particles exceeding the lowest detection limit of the APS.

The mass of aqueous trehalose delivered to APS_{wet} in 1 second reproducibly measures 4 μg, which is higher than that of mannitol (Fig. 5). This difference is explained by two key factors. Firstly, the RH in the APS_{wet} for trehalose (98 ± 1%) is higher than that for mannitol (95 ± 1%). This 3% difference in RH significantly affects the rGF in this RH range and the condensed phase mass of the aerosol. Secondly, the higher concentration of trehalose promotes more agglomeration, leading

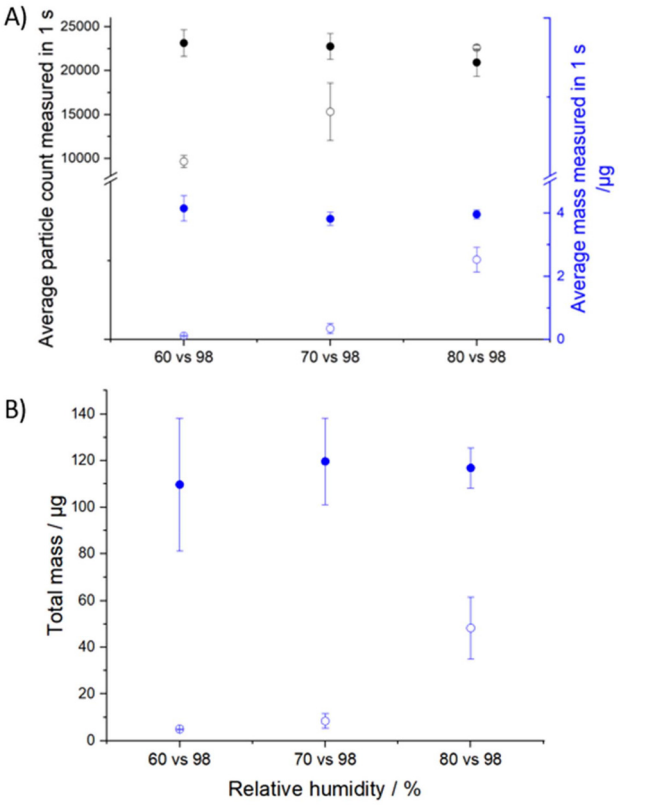

Fig. 7 (A) 5% w/w trehalose CHAPS results with 3 seconds of actuation for a range of RHs in the APS_{dry} from 80% down to 60%, while maintaining around 98 ± 1% in the APS_{wet} (n = 3 for each RH pair). The black symbols show the average particle count of the samples over 3 seconds. The blue symbols show the average mass over those 3 seconds. APS_{dry} data are presented using open dots, while APS_{wet} data are presented using filled dots. (B) Graph showing the cumulative mass of 5% w/w trehalose throughout the entire actuation with APS_{dry} shown in open dots and APS_{wet} in filled dots.

to the formation of larger particles and an increase in the average mass of trehalose particles.

In APS_{dry}, when the RH is at 60 ± 1%, a considerable amount of particles are lost below the detection limit and those that are sized by the APS are relatively small and carry limited mass. As the RH increases to 70 ± 1%, a minor rise in average mass is observed. When the RH reaches 80%, there is a substantial increase in particle mass due to hygroscopic growth tending towards that of APS_{wet} (Fig. 7A).

The total mass of trehalose particles entering the APS_{wet} is around 110 μg (Fig. 7B). The total mass in APS_{dry}, on the other hand, shows an increasing trend as the RH increases, from 3 μg at 60 ± 1% RH to 50 μg at 80 ± 1% (Fig. 7B). The increase in total mass is associated with the hygroscopic growth as shown in the rGF curve and amplified due to the cubic relationship between the particle radius and mass.

3.4. Hygroscopic plume dynamics for aerosolized aqueous salbutamol sulphate

A salbutamol sulphate molecule contains several polar functional groups including the hydroxyl and the amino groups (Fig. S7†). Davidson *et al.*[39] have demonstrated significant hygroscopicity of salbutamol sulphate at its deliquescence RH of ~92%.

3.4.1. Single particle characterization. The CK-EDB data for salbutamol sulfate (Fig. S8†) indicate greater hygroscopicity compared to mannitol and trehalose at water activity levels below 0.95. Beyond 0.95 water activity, the rGF of salbutamol sulphate increases exponentially. Due to the modelling limitations of the AIOMFAC model, sulphate ions could not be incorporated into the salbutamol model, hindering the conversion to the aerodynamic diameter. Consequently, only the geometric rGF derived from CK-EDB will be utilized to characterize the single droplet dynamics of salbutamol sulphate. According to the phase function data from the CK-EDB output (Fig. S9†), there are indications of crystallinity in the levitated droplet upon equilibration at 55% RH. Under RH conditions above 65%, the droplet remains homogeneous upon reaching equilibrium and can be assumed to be spherical.

3.4.2. Plume characteristics. The $rGFr_{aero}$ of 0.1% w/w aqueous salbutamol sulphate obtained from CHAPS is compared against that of the $rGFr_{geo}$ based on the CK-EDB output in Fig. 8. For this experiment, APS_{dry} covers RH ranges from 60 ± 1% to 90 ± 1%, while APS_{wet} maintains an RH of 96 ± 1%. Overall, CHAPS $rGFr_{aero}$ shows good agreement with EDB $rGFr_{geo}$ within the error range, as illustrated in Fig. 8.

Fig. 9A illustrates the cumulative particle count and mass of nebulized salbutamol sulphate per second during the interval of the first 3 stable seconds. In APS_{wet}, with RH maintained at 96%, the average particle count consistently measures just under 20 000 particles per second (Fig. 9A). In contrast, in APS_{dry} at 60 ± 1%, the particle count falls below 10 000, indicating a significant reduction, as many particles do not meet the detection threshold. However, when the RH reaches 70%, the particle count in APS_{dry} recovers to the same level as that of APS_{wet}. Although similar trends are observed for mannitol

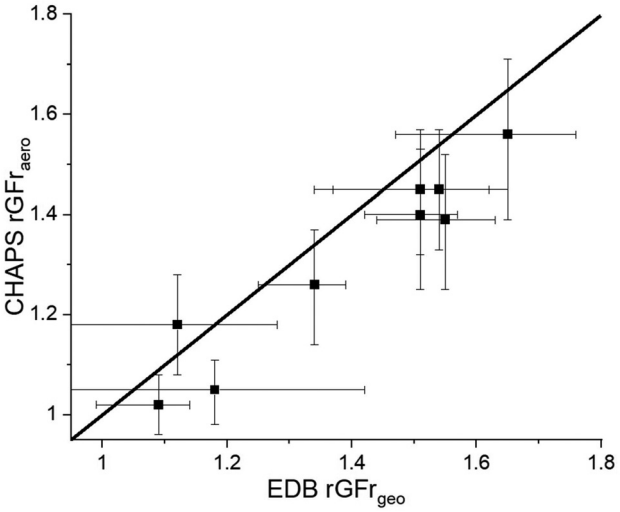

Fig. 8 Comparison between the CK-EDB $rGFr_{geo}$ and the CHAPS $rGFr_{aero}$ of aqueous salbutamol sulphate.

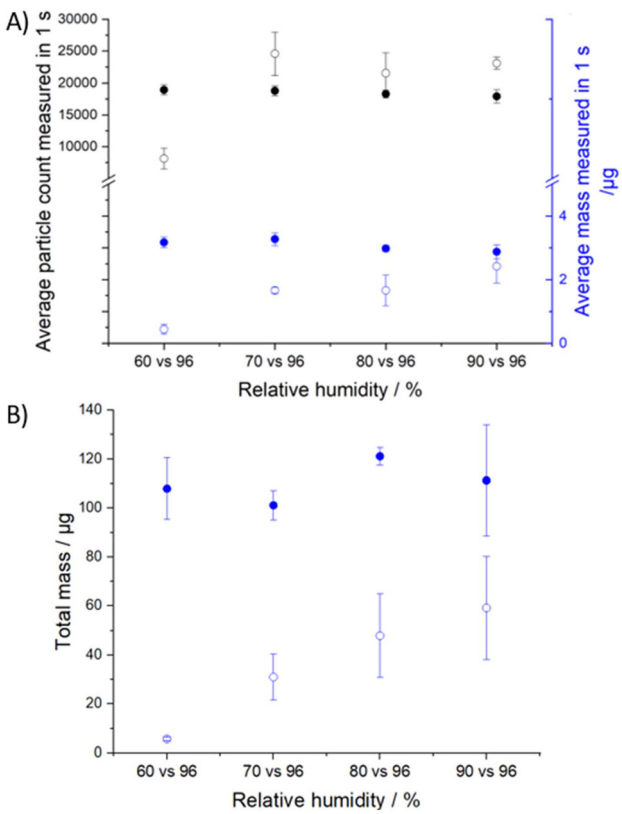

Fig. 9 (A) 0.1% w/w salbutamol sulphate CHAPS results with 3 seconds of actuation for a range of RHs in the APS_{dry} from 90% down to 60%, while maintaining around 96% ± 1% in the APS_{wet} (n = 3 for each RH pair). The black symbols show the average particle count of the samples over 3 seconds. The blue symbols show the average mass over those 3 seconds. APS_{dry} data are presented using open dots, while APS_{wet} data are presented using filled dots. (B) Graph showing the cumulative mass of 1% w/w salbutamol sulphate of the entire actuation with APS_{dry} shown in open dots and APS_{wet} in filled dots.

and trehalose, salbutamol exhibits a more pronounced increase in particle count over a narrower RH range. This effect is likely due to the higher hygroscopicity of salbutamol at lower humidity levels. The average particle count in APS_{dry} reproducibly measures ~22 500 from 70% to 90% RH (Fig. 9A), which suggests that most particles are above the detection threshold. The change in the RH continues to influence the size distribution of the plume in APS_{dry}, as evidenced by the varying rGFr values shown in Fig. 9A. The average mass delivered in 1 second in APS_{wet} remains around 3 μg at 96 ± 1% RH showing good reproducibility between actuations (Fig. 9A). For APS_{dry}, the mass gradually increases from ~0.5 μg at 60 ± 1% RH and reaches over 2 μg at 90 ± 1% RH.

The total mass measured by the APS_{wet} consistently falls around 110 μg (Fig. 9B) with some fluctuations likely due to the manual process of actuating the nebulizer. The total mass in APS_{dry} increased from ~5 μg at 60 ± 1% RH to ~60 μg at 90 ± 1% almost linearly, which agrees with the high sensitivity to the water content of salbutamol (Fig. S7†).

3.5. Hygroscopic plume dynamics for aerosolized aqueous tobramycin

Tobramycin in dry powder form is classified as hygroscopic, necessitating additional storage precautions.[14] The molecule contains multiple amino and hydroxyl groups, along with glycosidic linkages (Fig. S10†). In a previous study, Haddrell *et al.*[24] demonstrated that nebulized tobramycin exhibits an increase in radius as a function of RH. For this study, a 6% w/w tobramycin solution is prepared for CK-EDB and CHAPS measurements.

3.5.1. Single particle characterization. The CK-EDB rGF_{geo} curve (Fig. S11†) reveals that exponential growth in particle size begins around 0.85 water activity. Below this threshold, the gradient of the rGF_{geo} values remains relatively flat compared to that of salbutamol. Based on the EDB rGF_{geo} curves, tobramycin demonstrates a lower hygroscopicity than salbutamol. It is not possible to estimate the relationship between the MFS and water activity for tobramycin with the AIOMFAC model. Therefore, only the geometric rGF will be utilized for further analysis and comparisons.

3.5.2. Plume characteristics. Fig. 10 shows a comparison of the CK-EDB derived tobramycin single droplet $rGFr_{geo}$ against the CHAPS-based plume $rGFr_{aero}$. Similar to salbutamol, the phase function data for tobramycin (Fig. S12†) indicates signs of crystallization upon equilibration at 55% RH. Hence, the RH range in APS_{dry} is set between 65% and 85%. APS_{wet} maintains a constant RH of 97 ± 1% for comparison. Most of the data points in Fig. 11A† align with the gradient line indicating a good agreement between CHAPS and EDB measurements once again. This consistency suggests that both methods provide reliable and comparable results under the set environmental conditions.

In APS_{wet}, maintained at 97 ± 1% RH, the average particle count consistently measures just over 20 000 particles per second during the first 3 stable seconds (Fig. 11A). In APS_{dry}, the particle count increases from under 10 000 particles at

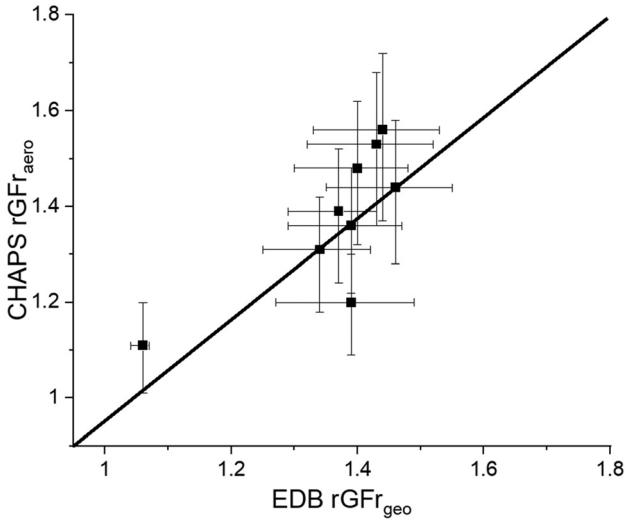

Fig. 10 Comparison between the CK-EDB $rGFr_{geo}$ and the CHAPS $rGFr_{aero}$ of aqueous tobramycin.

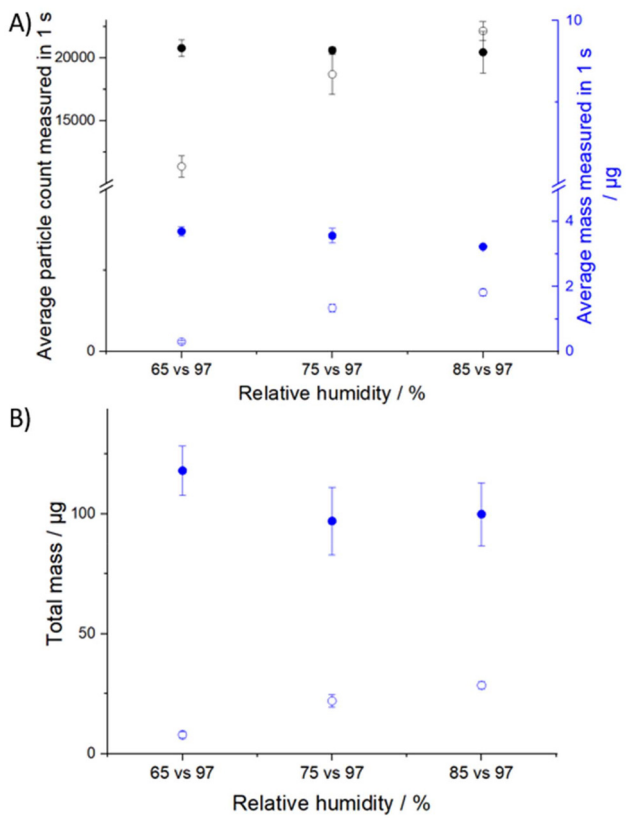

Fig. 11 (A) 6%w/w tobramycin CHAPS results with 3 seconds of actuation for a range of RHs in the APS_{dry} from 85% down to 65%, while maintaining around 97 ± 1% in the APS_{wet} (n = 3 for each RH pair). The black symbols show the average particle count of the samples over 3 seconds. The blue symbols show the average mass over those 3 seconds. APS_{dry} data are presented using open dots, while APS_{wet} data are presented using filled dots. (B) Graph showing the cumulative mass of tobramycin throughout the entire actuation with APS_{dry} (open dots) and APS_{wet} (filled dots).

65% RH to over 20 000 particles at 85% RH, converging on the value for APS_{wet}. This pattern is again likely due to the increasing number of particles surpassing the lower detection limit of the APS as a result of hygroscopic growth. In APS_{wet}, 3–4 μg of 6% w/w aqueous tobramycin aerosol is consistently delivered per second during the first 3 stable seconds. The average mass delivered in APS_{dry} is lower than in APS_{wet}, but gradually converges with APS_{wet} as the RH increases (Fig. 11A).

The total mass over the 3-second actuation of tobramycin in APS_{wet} measures ~100 μg (Fig. 11B). The total mass in APS_{dry} increased from ~8 μg at 65 ± 1%RH to ~30 μg at 85 ± 1% RH. The trend of increasing mass with an increase in RH conditions for tobramycin is consistent with the patterns observed in previously tested substances. Like other ingredients, tobramycin exhibits hygroscopic growth upon aerosolization, leading to greater mass at higher RH levels.

The CHAPS rGFr values are in strong agreement with those obtained using CK-EDB across various pharmaceutical ingredients. Additionally, as presented in Table 1, the CHAPS measurements exhibit high reproducibility for all tested compounds, demonstrating consistent particle counts and mass delivery at 96 ± 2% RH. The slight deviations in mass can likely be attributed to minor variations in RH during the experiments. APS_{wet} maintained the lowest RH (95%) for mannitol and the highest (98%) for trehalose, which is reflected in the corresponding mass differences. These variations may also be influenced by the intrinsic properties of the different compounds.

4. Comparison between CHAPS and next generation impactor size distributions for a typical inhaled formulation

The NGI is a conventional and accepted tool for the characterization of the aerosol particle size distribution from inhaled medications. It can be deployed for the measurement of nebules generated from a vibrating mesh nebulizer.[40] The NGI features 7 stages that allow for precise classification of the aerodynamic size distribution of particles.[41] Stage 1 corresponds to the largest cutoff diameter, while stage 7 corresponds to the smallest. In the experiments reported here, the NGI was kept in a ClimateZone™ (CTS, UK), which sets and controls the temperature and RH within the enclosure.[42] For consistency with the CHAPS procedures, the ClimateZone™ was set to maintain the temperature at 20 °C and with an RH set at either 50% or 96%.

Formulation X, a formulation provided by Chiesi, consists of multiple pharmaceutical active ingredients and is used to assess the performance of CHAPS against the NGI method for a typical inhalable formulation. A 10 mg ml^{-1} aqueous solution of Formulation X is actuated for 10 seconds from the Omron nebulizers for both NGI and CHAPS testing. The extended actuation time ensures that a sufficient number of particles reach the NGI stages, enabling the generation of a clear size distribution pattern. The APS categorizes particles into 52 size bins, ranging from 0.5 to 20 μm,[43] whereas the NGI has 7 stages, capable of covering particle sizes from below 0.5 μm to over 15 μm, depending on the flow rate.[41] The cutoff diameters of the NGI for nebulized Formulation X are provided in Table S1,† and the APS size bins have been combined to correspond to the particle size ranges covered by each NGI stage.

Fig. 12 illustrates the mass percentage distribution of the emitted dose across all NGI stages compared to the corresponding CHAPS size bins, which have been grouped to align with the bin widths of the NGI stages in both low (50%) and high (96%) RH environments. The comparison is presented using mass percentage rather than absolute mass because of the fundamental differences in how the NGI and CHAPS record mass. The NGI combined with high performance liquid chromatography analysis quantifies the mass of the solute alone, whereas CHAPS measures the mass of the entire droplets, including both the solute and solvent. Hence, it is necessary to use a normalized metric, such as mass percentage, to facilitate a meaningful comparison between the two instruments.

At 50% RH (left panel), the NGI data (orange bars) show an increase in deposition at stages 5 and 6, which suggests that there is a larger proportion of smaller particles under drier conditions. At 96% RH (right panel), the deposition profile shifts to the left, with a higher mass percentage in stages 2–4. The higher recovery in earlier stages is indicative of hygroscopic effects in high humidity leading to particle growth. The CHAPS data (blue bars) present a similar shift in the deposition profile to the NGI under both RH conditions.

The standard error in the NGI data is larger compared to CHAPS. The larger SEM observed in the NGI data may be attributed to the shorter actuation duration used in this method. Typically, nebulizer runs with NGIs require 10–30 minutes of actuation to minimize variability and achieve smaller SEM values. In this study, a shorter 10-second actuation was used, potentially leading to increased fluctuations in the data. In contrast, CHAPS consistently achieves reproducible results with actuation times as short as 3 seconds. Using CHAPS can be an efficient approach for screening a large number of samples for rapid preliminary assessments. Once the desired aerosol characteristics are identified, the NGI can

Table 1 Reproducibility of particle count and mass delivered per second by CHAPS APS_{wet} at 96 ± 2% RH for different pharmaceutical ingredients

96 ± 2% RH	Average particle count per second	Standard deviation of particle count	Mass delivered per second (μg)	Standard deviation of mass
Mannitol	18 056	1695	2.478	0.2
Salbutamol	18 552	912	3.11	0.247
Trehalose	22 091	1667	3.978	0.263
Tobramycin	20 635	1575	3.489	0.316

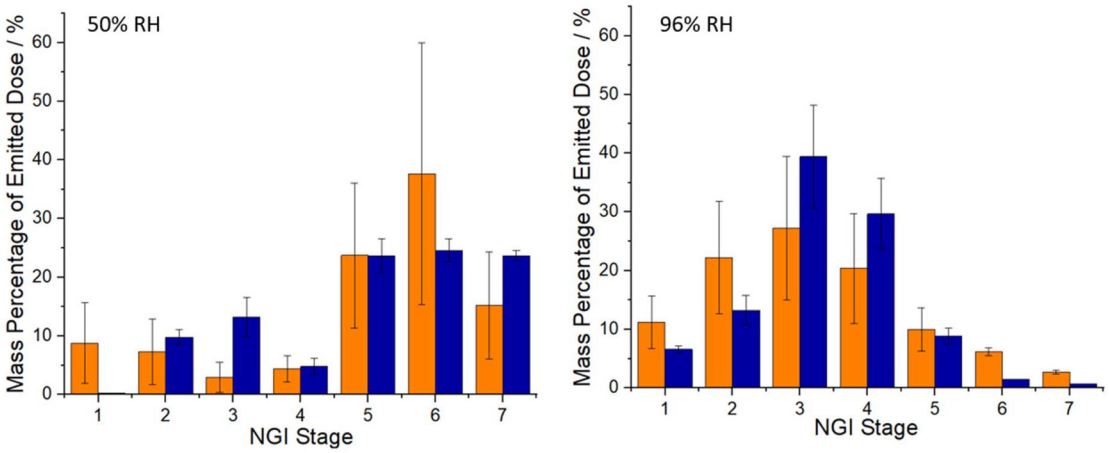

Fig. 12 Deposition profile of Formulation X emitted from a Respimat® SMI device at 20 °C using the NGI (orange) and CHAPS (blue) at 50 ± 1% RH and 96 ± 1% RH. Data are expressed as mean ± SEM, n = 3.

be used for detailed analysis, as it remains the industry standard for comprehensive aerodynamic particle size distribution and regulatory compliance. This two-step strategy can optimize workflow by combining the high-throughput capabilities of CHAPS with the rigorous validation provided by the NGI.

5. Conclusion

To understand and optimize the drug deposition profile of nebulized inhaled medicines, it is crucial to fully comprehend the aerosol dynamics of the plume. In this study, we present a novel approach for measuring the aerosol dynamics of various aqueous solutions generated *via* a nebulizer and demonstrate that RH affects the size distribution of the plume. The magnitude of the RH effect depends on the hygroscopicity of the ingredient. Additionally, the particle growth also increases exponentially as the RH surpasses 95%. The particle count and mass measured by CHAPS are reproducible. We also show that the rGFr values obtained from CHAPS are in alignment with those calculated from CK-EDB. These results suggest that single droplet characterization can be compared with plume measurements.

We have also demonstrated that CHAPS and NGI results exhibit similar trends under different RH conditions. However, it is important to recognize the differences in how these techniques establish deposition profiles, and selecting the appropriate method depends on the specific research objectives. For example, the NGI is more widely referenced in the literature, making it easier to benchmark and compare results. Additionally, while the NGI is capable of capturing smaller particles that may fall below the detection limit of CHAPS, these smaller particles contribute minimally to the overall mass and are unlikely to have a significant impact on the total mass delivered. On the other hand, CHAPS offers a unique advantage with its time-sensitive output, allowing for detailed investigations of plume development in real time. In contrast, the NGI provides a comprehensive particle size distribution for the entire sample. By combining CHAPS and the NGI, a more complete approach for aerosol particle analysis is achieved, with CHAPS delivering high-resolution aerodynamic size data in real time, while the NGI offers a robust and established method for overall size distribution analysis.

Data availability

Data are available at the University of Bristol data repository, data.bris, at **https://doi.org/10.5523/bris.3rxizodvo4y1921v9lpgtcnwhb**.

Conflicts of interest

There are no conflicts to declare.

Acknowledgements

This research was funded by the EPSRC Aerosol Science Centre for Doctoral Training (grant code: EP/S023593/1). The research was also funded by Chiesi Farmaceutici SpA.

References

1 R. Dhand, M. Dolovich, B. Chipps, T. R. Myers, R. Restrepo and J. Rosen Farrar, The, Role of Nebulized Therapy in the Management of COPD: Evidence and Recommendations, *COPD J. Chronic Obstr. Pulm. Dis.*, 2012, **9**, 58–72, DOI: **10.3109/15412555.2011.630047**.

2 I. Khan, S. Yousaf, M. A. Alhnan, W. Ahmed, A. Elhissi and M. J. Jackson, Design Characteristics of Inhaler Devices Used for Pulmonary Delivery of Medical Aerosols, in *Surg.*

Tools Med. Devices, Second Ed, 2016, pp. 573–591. DOI: 10.1007/978-3-319-33489-9_19.

3 W. Longest, B. Spence and M. Hindle, Devices for Improved Delivery of Nebulized Pharmaceutical Aerosols to the Lungs, *J. Aerosol Med. Pulm. Drug Delivery*, 2019, **32**, 317, DOI: 10.1089/JAMP.2018.1508.

4 B. L. Laube, Aerosolized Medications for Gene and Peptide Therapy, *Respir. Care*, 2015, **60**, 806–821, DOI: 10.4187/respcare.03554.

5 A. Arı, Jet, Ultrasonic, and Mesh Nebulizers: An Evaluation of Nebulizers for Better Clinical Outcomes, *Eurasian J. Pulmonol.*, 2014, **16**, 1–7, DOI: 10.5152/ejp.2014.00087.

6 A. Ari, A. D. De Andrade, M. Sheard, B. Alhamad and J. B. Fink, Performance Comparisons of Jet and Mesh Nebulizers Using Different Interfaces in Simulated Spontaneously Breathing Adults and Children, *J. Aerosol Med. Pulm. Drug Delivery*, 2015, **28**, 281–289, DOI: 10.1089/JAMP.2014.1149.

7 R. Nave and H. Mueller, From Inhaler to Lung: Clinical Implications of the Formulations of Ciclesonide and Other Inhaled Corticosteroids, *Int. J. Gen. Med.*, 2013, **6**, 99–107, DOI: 10.2147/IJGM.S39134.

8 P. Sheth, S. W. Stein and P. B. Myrdal, Factors Influencing Aerodynamic Particle Size Distribution of Suspension Pressurized Metered Dose Inhalers, *AAPS PharmSciTech*, 2015, **16**, 192, DOI: 10.1208/S12249-014-0210-Z.

9 A. J. Hickey and T. B. Martonen, Behavior of Hygroscopic Pharmaceutical Aerosols and the Influence of Hydrophobic Additives, *Pharm. Res.*, 1993, **10**, 1–7, DOI: 10.1023/a:1018952425107.

10 R. D. Restrepo and B. K. Walsh, Humidification during Invasive and Noninvasive Mechanical Ventilation: 2012, *Respir. Care*, 2012, **57**, 782–788, DOI: 10.4187/respcare.01766.

11 Inspiring Available online: https://www.irdd.com.au/ (accessed on 27 June 2024).

12 A. Zuend, C. Marcolli, T. Peter and J. H. Seinfeld, AIOMFAC Available online: https://www.aiomfac.caltech.edu.

13 A. Sverrild, C. Porsbjerg and V. Backer, The Use of Inhaled Mannitol in the Diagnosis and Management of Asthma, *Respir. Res.*, 2011, **13**, 115–123, DOI: 10.1517/14656566.2012.638917.

14 D. R. Vandevanter and D. E. Geller, Tobramycin Administered by the TOBi ® Podhaler ® for Persons with Cystic Fibrosis: A Review, *Med. Devices: Evidence Res.*, 2011, 4–179, DOI: 10.2147/MDER.S16360.

15 K. B. J. Beswick, G. M. Pover and S. Sampson, Long-Term Regularly Inhaled Salbutamol, *Curr. Med. Res. Opin.*, 1986, **10**, 228–234, DOI: 10.1185/03007998609110443.

16 S. Ohtake and Y. J. Wang, Trehalose: Current Use and Future Applications, *J. Pharm. Sci.*, 2011, **100**, 2020–2053, DOI: 10.1002/JPS.22458.

17 G. Rovelli, R. E. H. Miles, J. P. Reid and S. L. Clegg, Accurate Measurements of Aerosol Hygroscopic Growth over a Wide Range in Relative Humidity, *J. Phys. Chem. A*, 2016, **120**, 4376–4388, DOI: 10.1021/acs.jpca.6b04194.

18 J. F. Davies, A. E. Haddrell and J. P. Reid, Time-Resolved Measurements of the Evaporation of Volatile Components from Single Aerosol Droplets, *Aerosol Sci. Technol.*, 2012, **46**, 666–677, DOI: 10.1080/02786826.2011.652750.

19 A. Haddrell, G. Rovelli, D. Lewis, T. Church and J. Reid, Identifying Time-Dependent Changes in the Morphology of an Individual Aerosol Particle from Its Light Scattering Pattern, *Aerosol Sci. Technol.*, 2019, **53**, 1334–1351, DOI: 10.1080/02786826.2019.1661351.

20 J. S. Walker, J. Archer, F. K. A. Gregson, S. E. S. Michel, B. R. Bzdek and J. P. Reid, Accurate Representations of the Microphysical Processes Occurring during the Transport of Exhaled Aerosols and Droplets, *ACS Cent. Sci.*, 2021, **7**, 200–209, DOI: 10.1021/ACSCENTSCI.0C01522/SUPPL_FILE/OC0C01522_SI_002.PDF.

21 A. E. Haddrell, J. F. Davies, L. A. Dailey, D. Murnane and J. P. Reid, A Detailed Understanding of Physicochemical Properties of Pharmaceutical Containing Aerosol Can Be Used to Improve Targeted Drug Delivery in the Lung.; Drug Delivery to the Lungs conference, 2016.

22 D. A. Hardy, J. F. Robinson, T. G. Hilditch, E. Neal, P. Lemaitre, J. S. Walker and J. P. Reid, Accurate Measurements and Simulations of the Evaporation and Trajectories of Individual Solution Droplets, *J. Phys. Chem. B*, 2023, **127**, 3430, DOI: 10.1021/acs.jpcb.2c08909.

23 Y. Huang, A. A. Adebiyi, P. Formenti and J. F. Kok, ., Linking the Different Diameter Types of Aspherical Desert Dust Indicates That Models Underestimate Coarse Dust Emission, *Geophys. Res. Lett.*, 2021, **48**, 1–12, DOI: 10.1029/2020GL092054.

24 A. E. Haddrell, J. F. Davies, R. E. H. Miles, J. P. Reid, L. A. Dailey and D. Murnane, Dynamics of Aerosol Size during Inhalation: Hygroscopic Growth of Commercial Nebulizer Formulations, *Int. J. Pharm.*, 2014, **463**, 50–61, DOI: 10.1016/j.ijpharm.2013.12.048.

25 A. Zuend, C. Marcolli, A. M. Booth, D. M. Lienhard, V. Soonsin, U. K. Krieger, D. O. Topping, G. McFiggans, T. Peter and J. H. Seinfeld, Atmospheric Chemistry and Physics New and Extended Parameterization of the Thermodynamic Model AIOMFAC: Calculation of Activity Coefficients for Organic-Inorganic Mixtures Containing Carboxyl, Hydroxyl, Carbonyl, Ether, Ester, Alkenyl, Alkyl, and Aromatic Functional Groups, *Atmos. Chem. Phys.*, 2011, **11**, 9155–9206, DOI: 10.5194/acp-11-9155-2011.

26 A. Zuend, C. Marcolli, T. Peter and J. H. Seinfeld, Computation of Liquid-Liquid Equilibria and Phase Stabilities: Implications for RH-Dependent Gas/Particle Partitioning of Organic-Inorganic Aerosols, *Atmos. Chem. Phys.*, 2010, **10**, 7795–7820, DOI: 10.5194/acp-10-7795-2010.

27 Y. L. Jiang, A. D. Hardy, R. J. Ruiz, R. Friend and P. J. Reid, Comparative Time-Resolved Measurements of Aerosol Plume Size Distributions at Two Relative Humidities Using a Tandem Aerodynamic Particle Sizer Approach, *Aerosol Sci. Technol.*, 2025, DOI: 10.1080/02786826.2025.2486333.

28 Y. Yang, J. Liu, A. Hu, T. Nie, Z. Cheng and W. Liu, A Critical Review on Engineering of D-Mannitol Crystals:

Properties, Applications, and Polymorphic Control, *Crystals*, 2022, **12**(8), 1080, DOI: **10.3390/cryst12081080**.

29 Mannitol: Uses, Interactions, Mechanism of Action | DrugBank Online Available online: **https://go.drugbank.com/drugs/DB00742** (accessed on 15 May 2024).

30 S. J. Nevitt, J. Thornton, C. S. Murray and T. Dwyer, Inhaled Mannitol for Cystic Fibrosis, *Cochrane Database Syst. Rev.*, 2020, **5**(5), CD008649, DOI: **10.1002/14651858.CD008649.pub4**.

31 C. Koch and N. Høiby, Pathogenesis of Cystic Fibrosis, *Lancet*, 1993, **341**, 1065–1069, DOI: **10.1016/0140-6736(93)92422-p**.

32 J. C. Davies, Pseudomonas Aeruginosa in Cystic Fibrosis: Pathogenesis and Persistence, *Paediatr. Respir. Rev.*, 2002, **3**(2), 128–134, DOI: **10.1016/S1526±0550(02)00003-3**.

33 D. Bilton, E. Daviskas, S. Anderson, J. Kolbe, G. King, G. R. Stirling, R. B. Thompson, D. Milne and B. Charlton, Phase 3 Randomized Study of the Effi Cacy and Safety of Inhaled Dry Powder Mannitol for the Symptomatic Treatment of Non-Cystic Fibrosis Bronchiectasis, *Chest*, 2013, **144**, 216–225.

34 Mannitol (Inhalation Route) Description and Brand Names - Mayo Clinic Available online: **https://www.mayoclinic.org/drugs-supplements/mannitol-inhalation-route/description/drg-20074757** (accessed on 15 May 2024).

35 S. Sadr, M. Kiani, M. Rezaei, G. Khanbabaee, S. A. Tabatabaee and A. Hosseini, The Efficacy of Nebulized Soluble Mannitol and Comparison with 5% Hypertonic Saline on Pulmonary Function of Children with Cystic Fibrosis, *J. Compr. Pediatr.*, 2019, **10**, DOI: **10.5812/COMPREPED.85616**.

36 M. Burek, S. Waskiewicz, I. Wandzik and K. Kaminska, Trehalose – Properties, Biosynthesis and Applications, *Chemik*, 2015, **69**, 473–476.

37 A. B. Richards, S. Krakowka, L. B. Dexter, H. Schmid, A. P. M. Wolterbeek, D. H. Waalkens-Berendsen, A. Shigoyuki and M. Kurimoto, Trehalose: A Review of Properties, History of Use and Human Tolerance, and Results of Multiple Safety Studies, *Food Chem. Toxicol.*, 2002, **40**, 871–898, DOI: **10.1016/S0278-6915(02)00011-X**.

38 N. C. A. Green, *Dynamic Response of Hygroscopic Pharmaceutical Aerosol on Inhalation*, University of Bristol, 2021.

39 N. Davidson, H. J. Tong, M. Kalberer, P. C. Seville, A. D. Ward, M. K. Kuimova and F. D. Pope, Measurement of the Raman Spectra and Hygroscopicity of Four Pharmaceutical Aerosols as They Travel from Pressurised Metered Dose Inhalers (PMDI) to a Model Lung, *Int. J. Pharm.*, 2017, **520**, 59–69, DOI: **10.1016/j.ijpharm.2017.01.051**.

40 J. G. Y. Chan, D. Traini, H. K. Chan, P. M. Young and P. C. L. Kwok, Delivery of High Solubility Polyols by Vibrating Mesh Nebulizer to Enhance Mucociliary Clearance, *J. Aerosol Med. Pulm. Drug Delivery*, 2012, **25**, 297–305, DOI: **10.1089/jamp.2011.0961**.

41 V. A. Marple, D. Hochrainer, D. L. Roberts, F. J. Romay, N. C. Miller, K. G. Truman, M. Van Oort, B. Olsson, M. J. Holroyd and J. P. Mitchell, Next Generation Pharmaceutical Impactor (A New Impactor for Pharmaceutical Inhaler Testing). Part I: Design, *J. Aerosol Med.*, 2004, **16**, 283–299, DOI: **10.1089/089426803769017659**, **https://www.liebertpub.com/jam**.

42 ClimateZoneTM Enclosure – Climatically Controlled Enclosure available online: **https://containment-technology.co.uk/product/climatezone-enclosure/** (accessed on 21 August 2024).

43 Aerodynamic Particle Sizer APS 3321 | TSI Available online: **https://tsi.com/products/particle-sizers/supermicron-capable-particle-sizer-spectrometers/aerodynamic-particle-sizer-aps-3321/** (accessed on 21 August 2024).